- Technical Paper -

EFFECT OF SPECIFIC SURFACE AREA OF FIBER INCORPORATED IN CEMENTITIOUS COMPOSITES ON SHIELDING EFFECTIVENESS ACCORDING TO ELECTRICAL CONDUCTIVITY

Yaechan LEE[*1], Gyuyong KIM[*2], Sasui SASUI[*1] and Jeongsoo NAM[*2]

ABSTRACT

This study investigates the shielding effectiveness of concrete as protective properties. It is reported that the shielding effectiveness of electromagnetic pulsu(EMP) is closely related to electrical conductivity. Amorphous metallic fiber, smooth steel fiber, and hooked steel fiber were incorporated into cementitious composites to increase electrical conductivity, and the correlation between electrical conductivity and shielding effectiveness was analyzed. The results showed that the electrical conductivity of amorphous metallic fiber with large specific surface area was the highest, and the shielding effectiveness reached saturation after a certain critical point.

Keywords: electrical conductivity, shielding effectiveness, steel fiber, cementitious composites

1. INTRODUCTION

In recent years, geopolitical tensions and armed conflicts have contributed to a deteriorating international situation. The Russian-Ukrainian war, along with North Korea's sixth nuclear test and missile bombardment of the Eest Sea, has caused massive human and material damage around the world and raised awareness of potential risks. This situation has increased the need for protective blast protection of structures to protect critical infrastructure and mitigate potential damage.

However, cement composites, which are mainly used in structures, have high compressive strength, but low bending and tensile strength, resulting in brittle fracture characteristics. Therefore, high fracture energy is required to withstand rapid loads such as earthquakes, high-speed collisions, and explosions, and other measures are needed to ensure that cement composites with low fracture energy have excellent protective explosion protection performance. Previous studies have been conducted to increase the protective performance of cement composites by reinforcing them with various fiber[1–3].

On the other hand, North Korea recently conducted its sixth nuclear test and mentioned the possibility of an EMP attack using hydrogen bombs, so it is necessary to secure the performance of construction materials against various physical factors. However, cement-based materials, which are mainly used, have excellent compressive strength but are brittle, so they have poor crack control performance to withstand various loads, and low electrical conductivity, so it is difficult to expect shielding performance against electromagnetic radiation such as EMP (Electro Magnetic Pulse).

To improve this, research on fiber-reinforced cement composites is being continuously conducted to secure crack resistance performance by effectively controlling cracks in the cement matrix using crosslinking through fiber reinforcement, and to give electrical conductivity to cement-based materials by forming a conductive network using conductive steel fibers, carbon fibers[4].

However, in the case of general steel fibers, the weight of the structure is increased due to the high density, and there is a possibility that the crack resistance performance may be reduced by reducing the cross-linking effect of the fiber due to low corrosion resistance. In addition, it is difficult to construct a continuous conduction path due to the small specific surface area and high density. On the other hand, amorphous metallic fiber has a lower density compared to general steel fibers, which means that they can form a conductive network because they have a large number of inclusions at the same inclusion rate, excellent corrosion performance, and a thin plate with a large specific surface area.

However, existing studies have focused on the characteristics of these amorphous metallic fibers and evaluated the performance of amorphous metallic fiber reinforced cement composites only in terms of mechanical performance such as durability, mechanical properties, impact resistance, and fire resistance, and lack evaluation of electromagnetic properties such as electrical conductivity and electromagnetic wave shielding performance[5–13].

Therefore, this study evaluated the electrical conductivity and shielding effect of fiber-reinforced cement composites by reinforcing the cement composites with amorphous metallic fibers of two different lengths, smooth steel fibers with similar lengths, and hooked steel fibers. Through this study, the main characteristics of the fibers on the electrical conductivity of the fiber-reinforced cement composites and the correlation between the electrical conductivity and the shielding effect were compared and analyzed.

*1 Doctoral Course, Dept. of Architecture Engineering, Chungnam National University, JCI Member
*2 Prof., Dept. of Architecture Engineering, Chungnam National University, JCI Member

Table 3 Mix proportion

W/B	C/B	FA/B	S/B	Fibers (kg) (vol.%)	AF	SSF	HSF
0.4	0.85	0.15	0.35	0.5	36.0	39.3	
				1.0	72.0	78.5	
				1.5	108.0	117.8	
				2.0	144.0	157.2	

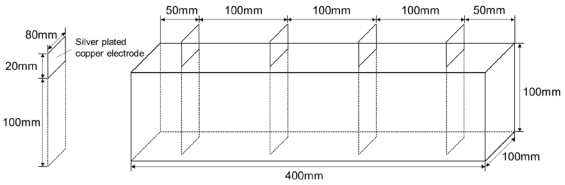

Fig.2 Specimen for electrical measurements

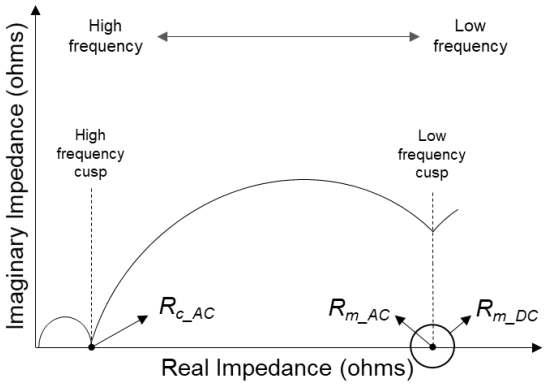

Fig.3 AC-IS response of FRCC

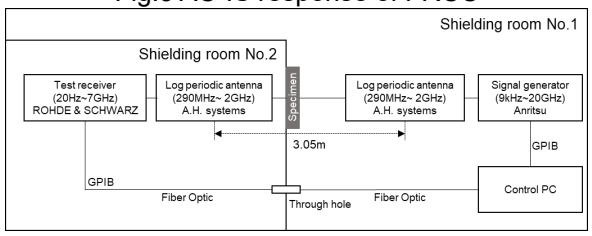

Fig.4 Electromagnetic shielding effectiveness measurements system

Table 1 Mechanical properties of the used fibers

Type	AF		SSF	HSF
Length (mm)	30	15	16.3	30
Diameter (mm)	0.25*1	0.25*1	0.2	0.5
Width (mm)	1.6	1.0	-	-
Thickness (μm)	29	24	-	-
Density (g/cm^3)	7.2	7.2	7.85	7.85
Specific surface area (m^2/kg)	11.6	9.6	2.6	1.0
Tensile strength (MPa)	1,400	1,400	2,600	1,140
Aspect ratio(L/D)	120	60	81.5	60
The number of fiber (/kg)	100,000	200,000	250,000	22,000

*1: Equivalent diameter

Table 2 Experimental plan

ID.	Type of fiber	Length (mm)	Fiber volume fraction (vol.%)
30AFRCC0.5	Amorphous metallic fiber	30	0.5
30AFRCC1.0			1.0
30AFRCC1.5			1.5
30AFRCC2.0			2.0
15AFRCC0.5		15	0.5
15AFRCC1.0			1.0
15AFRCC1.5			1.5
15AFRCC2.0			2.0
SSFRCC0.5	Smooth steel fiber	16.3	0.5
SSFRCC1.0			1.0
SSFRCC1.5			1.5
SSFRCC2.0			2.0
HSFRCC0.5	Hooked steel fiber	30	0.5
HSFRCC1.0			1.0
HSFRCC1.5			1.5
HSFRCC2.0			2.0

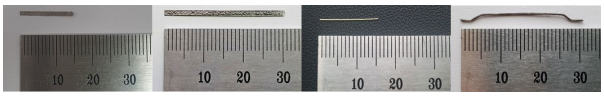

AF SSF HSF

Fig.1 Used fibers

2. TEST PROGRAMS

2.1 Materials and Mixture proportions

The physical properties and geometry of the fibers are shown in Table 1 and Fig. 1. Amorphous metallic fiber, hooked steel fibers, and smooth steel fibers all have Fe as the main component, and the proportion is higher for hooked steel fibers, smooth steel fibers, and amorphous metallic fibers.

The details of the test specimens in Table 2. The mix proportion of the fiber-reinforced cementitious composites in Table 3, and. The cement was one type of ordinary Portland cement, the water-reducing agent was a polycarbonate-based high-performance water-reducing agent, and the W/B was set to 0.4. Four types of fibers were incorporated into the test specimen: amorphous metallic fiber with a length of 30 mm, amorphous metallic fiber with a length of 15 mm, hooked steel fiber with a length of 30 mm, and smooth steel fiber with a length of 16.3 mm, and the incorporation rate was divided into 0.5, 1.0, 1.5 and 2.0 vol.%.

2.2 Preparation of specimens

To beam the steel fiber reinforced cementitious composite, the cement, fly ash, and silica sand were first dry beamed, then water and water-reducing agent were added to make a mortar, and then the fiber was added for sufficient beaming. After beaming, the fiber-reinforced cementitious composite was poured into the test mold, sealed, and cured in a constant temperature and humidity room for 1 day. The demolded specimens were then subjected to high temperature/steam curing at 90°C for 3 days, cooling at room temperature for 1 day, and drying at 60°C for 5 days to reduce the effect of moisture on electrical conductivity and shielding performance.

The test object for electrical conductivity evaluation was a cuboid with a length of 400 mm, width of 100 mm, and height of 100 mm, as shown in Fig. 2, and four electrodes were placed at 100 mm intervals using copper plates. The test body for EMP shielding p erformance evaluation was made of a cuboid with a width of 300 mm, a length of 300 mm, and a thickness of 100 mm.

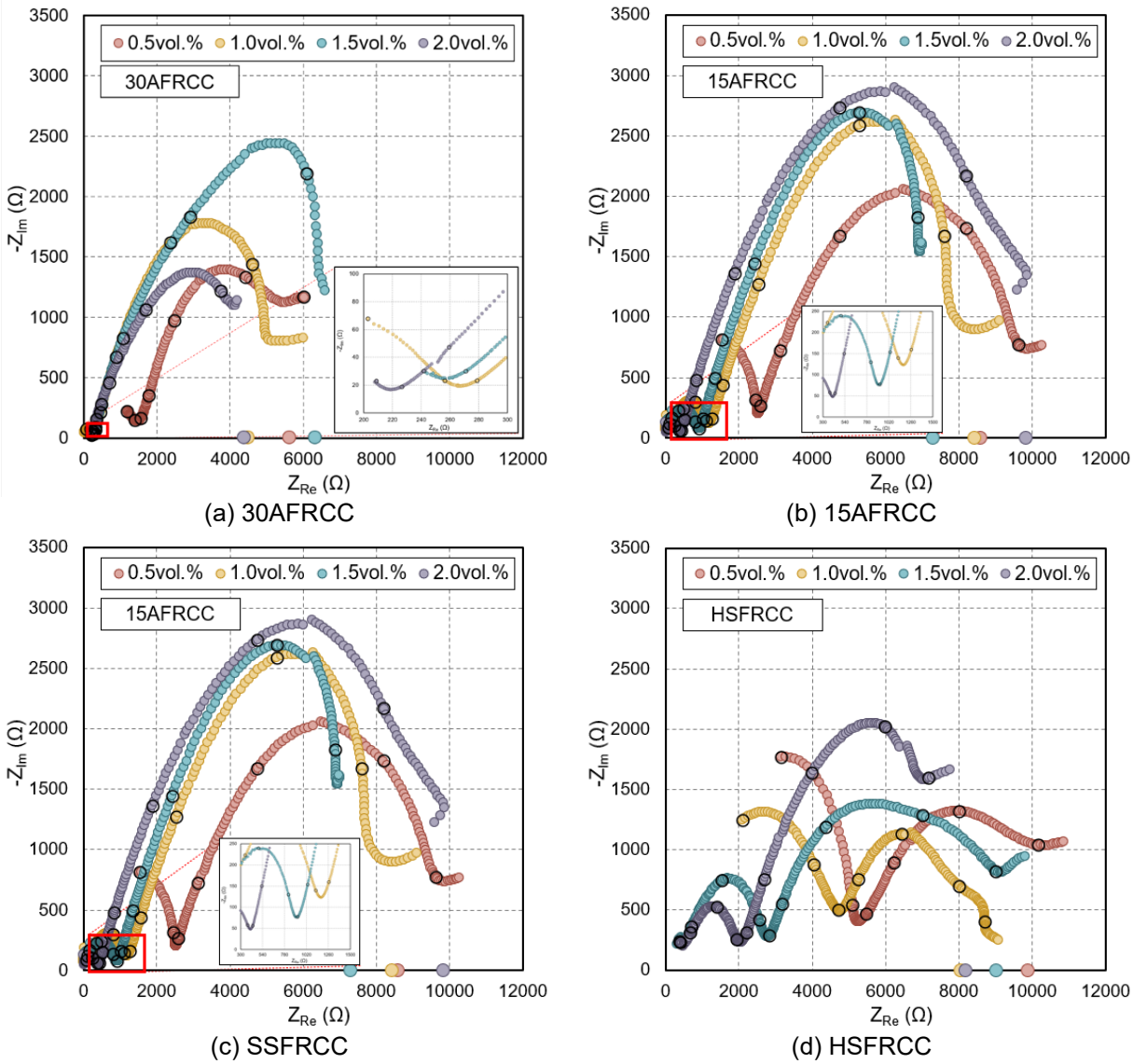

(a) 30AFRCC (b) 15AFRCC

(c) SSFRCC (d) HSFRCC

Fig.5 Nyquist plot

2.3 Experimental method

The electrical characterization was performed using a Princeton Applied Research PARSTAT 3000, first with EIS measurements and then with DC galvanodynamic measurements.

EIS measurements were performed using a four-probe method in which the working electrode and counter electrode leads are connected to the outer two electrodes of the four electrodes, and the reference electrode and sensing electrode leads are connected to the inner two electrodes, forcing a current from the outer electrode and evaluating the difference in voltage with the inner electrode. The frequency range was 1MHz~0.01mHz, the AC amplitude was 1000mV rms, and the measurement interval was set to logarithmic and 30 points per decade.

When the alternating current resistance of the steel fiber reinforced cement composite is measured by EIS measurement and plotted on the Nyquist plot, a dual arc is formed, as shown in Fig. 3, where two arcs are formed and then diverge, resulting in Rc_AC and Rm_AC. This is due to the fact that at low frequencies, the fiber is insulated and does not play a role, while at high frequencies, the fiber is short-circuited and current flows through the fiber. Rc_AC, which occurs at high frequencies, refers to the exchange of ionic current through the electrolyte and electronic current through the conductive fiber, while Rm_AC, which occurs at relatively low frequencies, refers to the resistance to ionic current passing through the pore solution acting as an electrolyte. Accordingly, Rm_DC, the resistance measured in DC, theoretically has the same value as Rm_AC.

To determine the DC resistance from the voltage-current curve, DC galvanodynamic measurements were performed, using four electrodes as in the EIS measurements. The current was increased at a constant rate of 50 μA/s at the external electrode, and the voltage increased directly proportionally with the overpotential and saturated, and then the voltage did not increase further even if the current was increased in the form of a curve. When deriving the DC resistance in this study, the resistance was derived in the initial state before reaching saturation.

The electrical conductivity(σ) of the test piece was obtained by the following equation.

$$\sigma\ (S/cm)=1/\rho=L/A\ 1/R \quad (1)$$

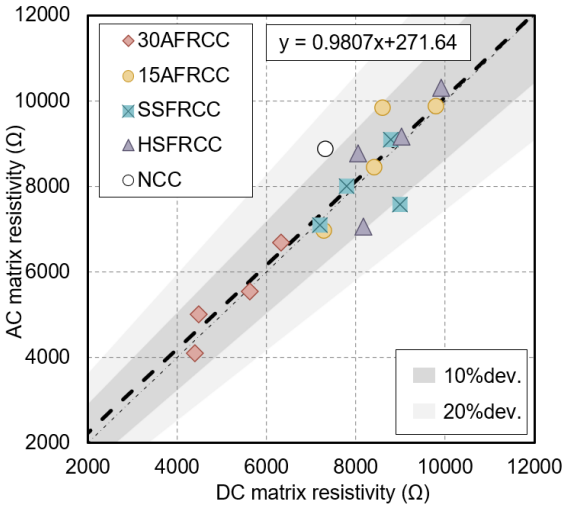

Fig.6 Comparison of AC matrix resistivity and DC matrix resistivity

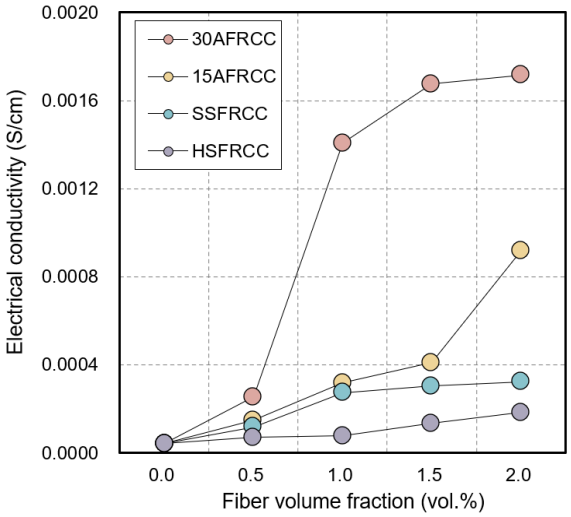

Fig.7 Electrical conductivity

where σ is the reciprocal of resistivity (ρ), electrical conductivity (S/cm), σ_{c_AC}, σ_{m_AC}, σ_{m_DC} are the electrical conductivities of composite$_{_AC}$, matrix$_{_AC}$, and matrix_DC, respectively, $Rc_{\_AC}$, $Rm_{\_AC}$, $Rm_{\_DC}$ are the electrical resistivity (Ω) of composite$_{_AC}$, matrix$_{_AC}$, and matrix$_{_DC}$, respectively, L is the distance between the electrodes (cm), and A is the area of the test piece parallel to the electrodes (cm^2).

The electromagnetic shielding effectiveness evaluation was measured according to the MIL-STD-188-125 standard, and the configuration of the measurement system is shown in Fig. 4. The antennas used for transmitting and receiving are log periodic antennas with a measurement frequency range of 290 MHz to 2 GHz. Shielding rooms 1 and 2 are separated by a metal wall, and the transmitting antenna is installed in shielding room 1 and the receiving antenna is installed in shielding room 2 at a distance of 3.05m, along the same line as the center of the opening of the test object mounting jig. The receiver was installed in shielding room 2 to reduce the influence of incoming electromagnetic waves, and the control PC and receiver were connected using optical cables.

The electromagnetic shielding effectiveness was obtained by the following equation.

$$SE(dB)=20 \log \frac{E_i}{E_t} \quad (2)$$

Where SE is the electromagnetic shielding effectiveness (dB), $E_{\_i}$ is the signal received without shielding, and $E_{\_t}$ is the signal received with shielding.

3. RESULTS AND DISCUSSION

3.1 Nyquist plot

The Nyquist plot for each test material is shown in Fig. 5, with the DC resistance on the y-axis. First, two arcs were formed in the case of the steel fiber reinforced cement composite with conductor as shown in Fig. 6, resulting in two vertices (R_{c_AC}, R_{m_AC}). In the case of R_{c_AC}, the electrical resistivity was evaluated to be lower as the percentage of fiber incorporation increased. When compared according to the fiber incorporation rate, it was found that R_{c_AC} decreased as the fiber incorporation rate increased.

3.2 Electrical conductivity

The R_{c_AC} resistance derived from the Nyquist line in Fig. 7 was introduced into Eq. 1 to derive the electrical conductivity. When compared by fiber incorporation rate, the electrical conductivity increased as the incorporation rate increased. Also, when compared by fiber type, 30AFRCC showed the highest electrical conductivity, followed by 15AFRCC, SSFRCC, and HSFRCC.

Depending on the type of fiber, 30 AFRCC is the highest, which is highly correlated with the specific surface area of the fiber and the number of fibers per weight. Compared to the hooked steel fiber with the same length as the amorphous metallic fiber of 30 mm, the specific surface area and fiber count per weight of the amorphous metallic fiber are 9.6 m^2/kg and 100,000 EA/kg, while the hooked steel fiber is 1.0 m^2/kg and 22,000 EA/kg, showing a high difference in specific surface area and fiber count per weight. In addition, when comparing 15 mm of amorphous metallic fibers with similar lengths of smooth steel fibers, the electrical conductivity of 15AFRCC was evaluated to be higher.

3.3 Shielding effectiveness

The shielding effect by frequency is shown in Fig. 8. The shielding test piece was measured twice in the horizontal and vertical directions, and the lower of the horizontal and vertical values was adopted for each frequency and plotted on the graph. Also, the average value of all frequencies was plotted as a straight line. The shielding effect was higher at low frequencies due to the size of the test piece.

The average shielding effectiveness values by frequency are plotted in Fig. 9. In the case of NCC, the lowest value of 16.4 dB was evaluated because it did not contain any conductors. The shielding effectiveness increased as the conductor inclusion rate increased, and the higher the percentage of fibers dispersed inside the matrix, the higher the shielding effectiveness. Also, depending on the type of fiber, 30 AFRCC, 15 AFRCC, SSFRCC, and HSFRCC were rated as the most effective, in order.

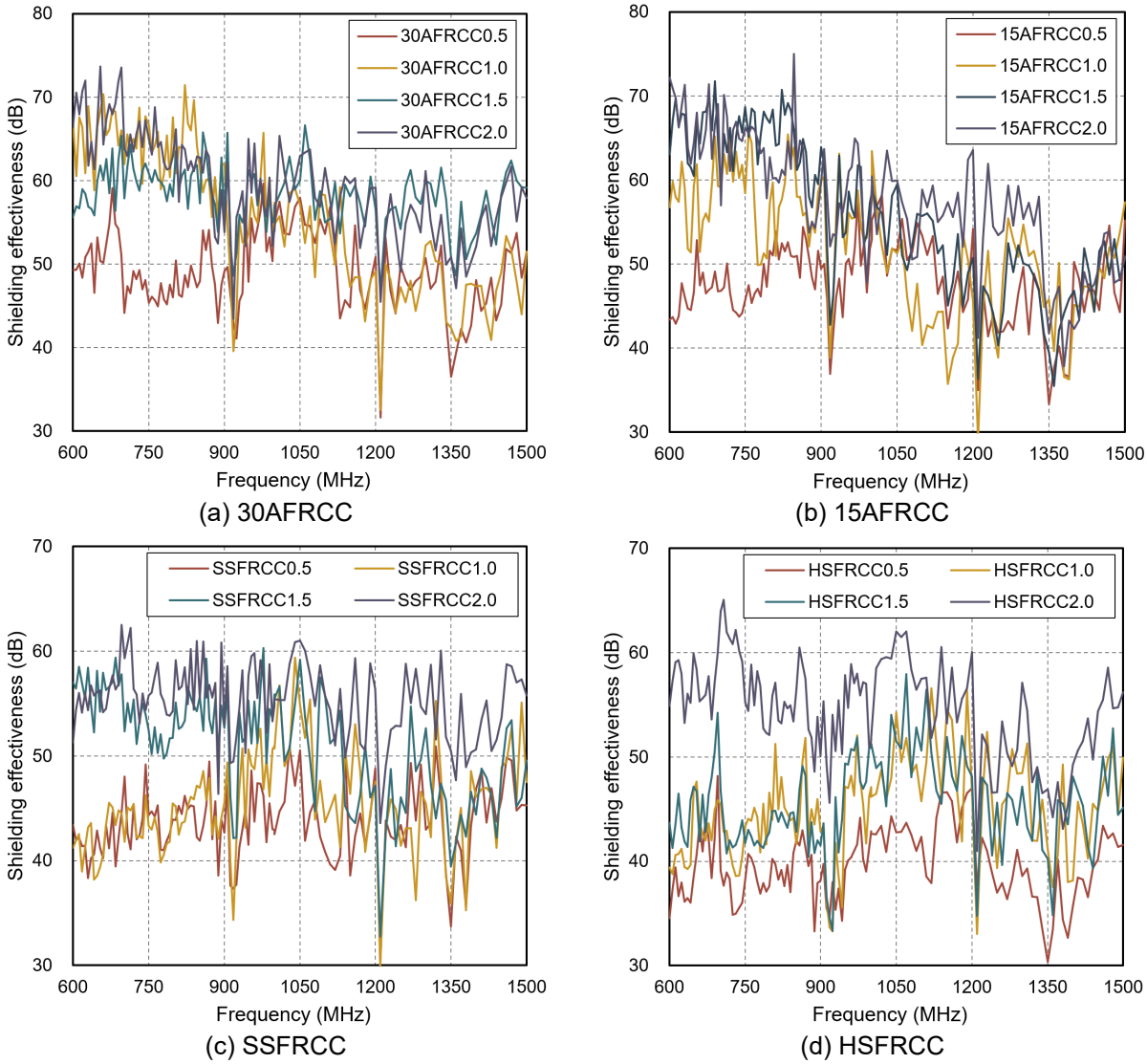

Fig.8 Shielding effectiveness

3.4 Correlation between electrical conductivity and shielding effectiveness

The correlation of the shielding effect according to the electrical conductivity of the test piece is shown in Fig. 10. As shown in the figure, the shielding effect tends to increase as the electrical conductivity of the fiber-reinforced cement composite increases. Accordingly, the correlation equation $y = 7.6366\ln(x) + 111.73$ is derived, and the approximate value of the shielding effect can be derived from the electrical conductivity of the fiber-reinforced cement composite.

However, as shown in the graph, it is observed that after 0.0004 S/sm, the shielding effect reaches a saturation state where the shielding effect does not increase. In previous papers, short length or powdered composites such as CNTs showed a direct relationship between electrical conductivity and shielding effectiveness, and the critical point due to the formation of conductive paths is also judged to be the same for electrical conductivity y and shielding effectiveness. However, in the case of the fiber-reinforced cement composite in this study, the critical point of electrical conductivity found in amorphous metallic fibers did not appear in the shielding effectiveness, and the shielding effectiveness also reached saturation. This is believed to be due to the fact that electromagnetic waves are converted into thermal energy through the steel fibers and scattered as they are incident on the shielding material, and further research is needed to determine the exact cause.

4. CONCLUSIONS

This study was conducted to evaluate the electrical conductivity and shielding effect of fiber-reinforced cement composites reinforced with amorphous metallic fibers, smooth steel fibers, and hooked steel fibers, and to compare and analyze their correlations, and the following results were obtained.

(1) When steel fibers are reinforced, it is believed that the specific surface area is a more dominant factor than the number of fibers, the electrical conductivity of the fibers themselves, or the aspect ratio that has the greatest impact on the shielding effect. Therefore, it is believed that thin, amorphous metallic fibers that can maintain a large specific surface area are more favorable for the formation of conductive paths than bedded fibers such as smooth steel fibers and hooked

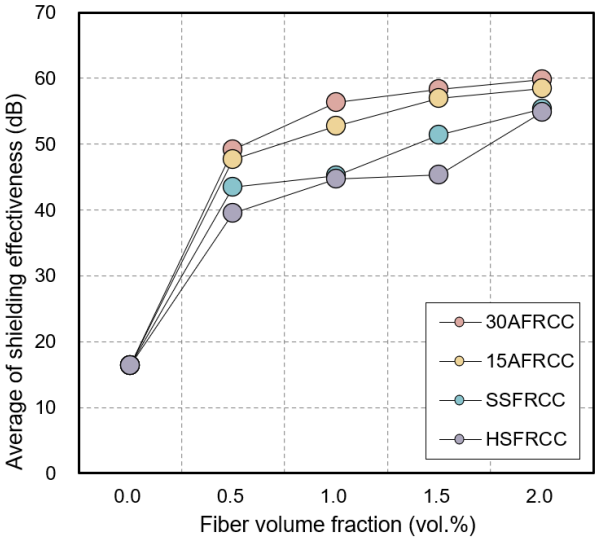

Fig.9 Average of shielding effectiveness

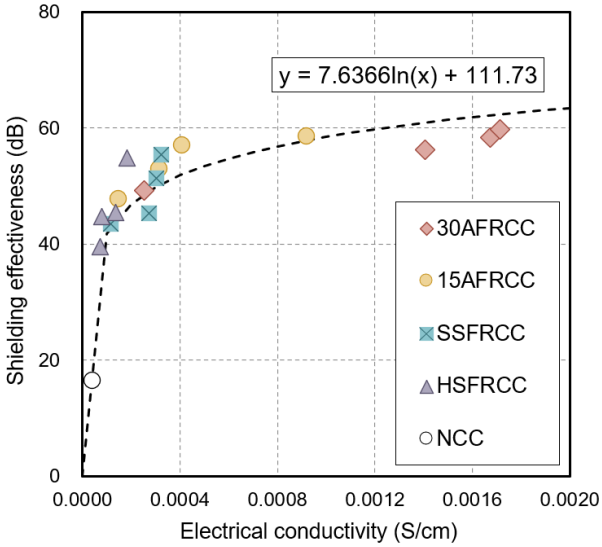

Fig.10 Correlating Shielding Effectiveness with Electrical Conductivity

steel fibers.

(2) The shielding effect of the fiber-reinforced cement composite was highly correlated with the electrical conductivity. It is believed that this result is due to the formation of a conductive path, which is the same as the electrical conductivity, as the shielding effect is converted into scattered and thermal energy by the conductor.

(3) In the case of the fiber-reinforced cement composite, due to the large gap between the fibers, it is believed that after 0.0004 S/cm, the shielding effect does not increase even if the electrical conductivity increases, and it is believed that this should be solved by increasing the contact resistance between the conductors.

ACKNOWLEDGEMENT

This work was supported by the National Research Foundation of Korea(NRF) grant funded by the Korea government(MSIT). (No. 2019R1A2C2085867)

REFERENCES

[1] H. Kim, G. Kim, S. Lee, M. Son, G. Choe, J. Nam, Strain rate effects on the compressive and tensile behavior of bundle-type polyamide fiber-reinforced cementitious composites, Compos. Part B Eng. 160 (2019) 50–65.

[2] M. Son, G. Kim, H. Kim, S. Lee, J. Nam, K. Kobayashi, Effects of the strain rate and fiber blending ratio on the tensile behavior of hooked steel fiber and polyvinyl alcohol fiber hybrid reinforced cementitious composites, Cem. Concr. Compos. 106 (2020).

[3] H. Kim, G. Kim, S. Lee, G. Choe, J. Nam, T. Noguchi, V. Mechtcherine, Effects of strain rate on the tensile behavior of cementitious composites made with amorphous metallic fiber, Cem. Concr. Compos. 108 (2020).

[4] S. Lee, G. Kim, H. Kim, M. Son, Y. Lee, Y. Choi, J. Woo, J. Nam, Electromagnetic wave shielding properties of amorphous metallic fiber-reinforced high-strength concrete using waveguides, Materials (Basel). 14 (2021).

[5] S. Lee, G. Kim, H. Kim, M. Son, G. Choe, K. Kobayashi, J. Nam, Impact resistance, flexural and tensile properties of amorphous metallic fiber-reinforced cementitious composites according to fiber length, Constr. Build. Mater. 271 (2021) 121872.

[6] H. Kim, G. Kim, S. Lee, G. Choe, T. Noguchi, J. Nam, Direct tensile behavior of amorphous metallic fiber-reinforced cementitious composites: Effect of fiber length, fiber volume fraction, and strain rate, Compos. Part B Eng. 177 (2019).

[7] H. Kim, G. Kim, J. Nam, J. Kim, S. Han, S. Lee, Static mechanical properties and impact resistance of amorphous metallic fiber-reinforced concrete, Compos. Struct. 134 (2015) 831–844.

[8] G. Choe, G. Kim, H. Kim, E. Hwang, S. Lee, J. Nam, Effect of amorphous metallic fiber on mechanical properties of high-strength concrete exposed to high-temperature, Constr. Build. Mater. 218 (2019) 448–456.

[9] G. Choe, G. Kim, H. Kim, E. Hwang, S. Lee, M. Son, J. Nam, Influence of amorphous metallic fibers on spalling properties of high-strength concrete exposed to high temperature, Constr. Build. Mater. 263 (2020) 120711.

[10] M.S. Kim, Structure and Properties of Amorphous Materials, J. Corros. Sci. Soc. Korea. 8 (1979) 24.

[11] Hwang, E., Kim, G., Koo, K., Moon, H., Choe, G., Suh, D., & Nam, J. (2021). Compressive creep and shrinkage of high-strength concrete based on limestone coarse aggregate applied to high-rise buildings. Materials, 14(17), 5026.

[12] Hwang, E., Kim, G., Choe, G., Yoon, M., Son, M., Suh, D., ... & Nam, J. (2021). Explosive spalling behavior of single-sided heated concrete according to compressive strength and heating rate. Materials, 14(20), 6023.

[13] Kang, B., Kim, G., Lee, T., Koo, K., Lee, S., Son, M., ... & Eu, H. (2022). Effects of Blast Furnace Slag Powder and Limestone Powder on the Mechanical Properties and Durability of Shotcrete Using Monocalcium Aluminate Setting Accelerator. Materials, 15(7), 2495.